Polarized-proton-induced exclusive pion production in ^{12}C at 200, 216, 225, 237, and 250 MeV incident energies

G. J. Lolos,* E. G. Auld, W. R. Falk,† G. L. Giles, G. Jones, B. J. McParland, R. B. Taylor,‡ and W. Ziegler
Physics Department, University of British Columbia, Vancouver, British Columbia, Canada V6T 2A6

P. L. Walden
TRIUMF, Vancouver, British Columbia, Canada V6T 2A3
(Received 31 January 1984)

The angular distributions of the differential cross sections and analyzing powers are presented for the $^{12}C(p,\pi^+)^{13}C^*$ reaction leading to the ground state of ^{13}C as well as some of the $^{13}C^*$ low-lying excited states. The analyzing powers for some of the transitions exhibit a considerable energy dependence while for other transitions they remain relatively unchanged, thus indicating a dynamic sensitivity of the analyzing power dependent on nuclear structure. Comparisons of theoretical predictions for A_{N0} and $d\sigma/d\Omega$, based on microscopic two-nucleon models, with our results indicate that substantial differences between theory and experiment still exist for $A(p,\pi^+)A+1$ type of reactions.

I. INTRODUCTION

The interest in exclusive pion production reactions of the type $pA \rightarrow \pi^+(A+1)$ has its origins in an important property of such reactions, namely the very large momentum transfer to the final nucleus. The (p,π) reaction was thus seen as a potentially valuable probe of high momentum components of the nuclear wave functions and as such the reaction promised to yield information on certain aspects of nuclear structure which are not readily accessible via most other reactions. As a result, reactions of this type have attracted considerable attention, experimental as well as theoretical, over the past several years with a number of review papers written on the subject.[1–3]

The early work at Uppsala on light nuclei[4–7] with unpolarized protons of 185 MeV concentrated on the measurement of angular distributions of differential cross sections for specific final states of the daughter nucleus. For some of the light nuclei investigated, the differential cross section clearly depended on the structure of the final nuclear configuration. Since then a wealth of experimental results has been accumulated for incident proton energies from threshold up to 800 MeV. At present, however, the quality of our current understanding of the reaction mechanism does not match that of the experimental results.[3] In fact, these measurements pointed out the necessity of understanding the reaction mechanism before any meaningful information on nuclear structure can be gleaned.

The first detailed polarization measurements on pion production from nuclei were performed at TRIUMF with ^9Be and ^{12}C as targets at 200 MeV.[8] The results were interesting on a qualitative level for two reasons:

(a) they indicated a "universal" characteristic for the angular distribution of the analyzing power $A_{N0}(\theta)$ [also frequently denoted by $A_y(\theta)$]; a common angular dependence characterized both nuclei and all the energy levels observed;

(b) the shape of $A_{N0}(\theta)$ was remarkably similar to that of the $\vec{p}p \rightarrow d\pi^+$ reaction when the appropriate kinematical corrections were applied.[9]

These polarization measurements introduced an additional constraint on the pion production theory. The most widely used model for the (p,π) reaction mechanism was based on a single nucleon model (SNM) in which the incoming proton interacts with the field of the nucleus, is stripped of its positive pion, and becomes a bound neutron. All the momentum transfer is then taken up by a single nucleon with neither the initial nor final nuclei entering explicitly into the interaction Hamiltonian. Such a model is obviously naive. A more sophisticated version involves the incorporation of distortions for both the proton and pion wave functions by the spectator nucleus. Optical potentials extracted from p-N and π-N scattering measurements are used to describe the distortions. Use of such a model[10] in a DWBA has met with limited success in fitting $d\sigma/d\Omega(\theta)$ and some $A_{N0}(\theta)$ results; however, as with all other theoretical approaches thus far, the model fails to simultaneously reproduce *both* the $d\sigma/d\Omega(\theta)$ and $A_{N0}(\theta)$ data. The universal nature of the first polarization measurements[8] indicated a reaction mechanism inconsistent with that of a simple SNM; rather the lack of nuclear structure sensitivity of the observed $A_{N0}(\theta)$ together with the fact that the angular dependence was similar to that of the elementary $pp \rightarrow d\pi^+$ reaction were suggestive of a production mechanism involving the interaction of at least two nucleons. Unfortunately, realistic pion production calculations based on such a two-nucleon model (TNM) have turned out to be very complicated. In the few cases where explicit TNM calculations have been performed, the fit to the $d\sigma/d\Omega(\theta)$ results is improved over those based on SNM calculations.[3] Only very recently, however, have predictions of $A_{N0}(\theta)$ [in addition to $d\sigma/d\Omega(\theta)$] using such a microscopic TNM been attempted.[11,12]

There currently exists in the literature a substantial

body of polarization data concerning exclusive pion production from light nuclei. These measurements were carried out mostly at the Indiana University Cyclotron Facility (IUCF) in the threshold to 200 MeV region[13–15] and at TRIUMF for protons in the range of 200–250 MeV.[16–20] No polarization results on light nuclei ($A > 2$) are available at higher energies. Unfortunately, no coherent picture of the (p,π) reaction has emerged thus far from these measurements. The original shape for the $A_{N0}(\theta)$ at 200 MeV (Ref. 8) appears to characterize all the reactions studied below 200 MeV (independent of both the target nucleus and the nature of the specific state excited) with but two exceptions, those of the $^{17}O_{0.87\ MeV}$ and $^{11}B_{4.45\ MeV}$ excited states.[14]

In the energy region from threshold to 200 MeV the angular distribution of the analyzing power is also seen to be independent of incident proton energy (where tested), while above 200 MeV (up to 250 MeV) it shows [at least for the case of the $^{12}C(\vec{p},\pi^+)^{13}C_{g.s.}$ reaction] a significant variation with increasing energy.[18] Such a strong energy dependence, however, is not shared by the transition to the $^{13}C_{9.50\ MeV}$ excited state which continues to exhibit the universal $A_{N0}(\theta)$ characteristic of all the other transitions observed below 200 MeV.[18,19] In comparison, the $^{9}Be(p,\pi^+)^{10}Be$ reaction shows no significant energy or state dependence in the same energy range.[17]

In this paper we present the angular distributions of the analyzing power and the differential cross section for incident proton energies of 200, 216, 225, 237, and 250 MeV. A description of the experimental apparatus and the method of analyzing the data is presented in Sec. II. The experimental results are presented and compared to the theory in Sec. III. Section IV contains the conclusions to be drawn from the data, together with suggested courses of action for the study of the $A(p,\pi^+)A+1$ reaction in the future.

II. EXPERIMENTAL

A. The beam

The experiment was performed at the TRIUMF cyclotron using an extracted polarized proton beam, the intensity of which was in the range of 20–30 nA for these measurements. The polarization was typically 75%.

The beam intensity as well as its polarization were monitored at different times by two polarimeters based on p-p elastic scattering from a thin CH_2 (polyethylene) target. Both polarimeters were detecting in coincidence the protons to both the left and the right of the direction of the beam (defining the recoil and scattered protons). The 200, 225, and 250 MeV results were obtained using a four-arm eight-counter polarimeter located upstream of the target location. The elastically scattered protons were detected at 26° (lab) while the recoil protons were detected at $-60°$ (lab) relative to the beam direction.[21] This polarimeter was replaced with an improved design for the 216 and 237 MeV results. The latter was a four-arm six-counter polarimeter which involved detection of the scattered protons at 17° (lab) and the recoil protons at $-73°$ (lab) relative to the beam direction.[22] The newer design provided greater physical rigidity to the counters; it had a larger analyzing power[23] and was less sensitive to beam spot location than the original design.

At the later stages of the experiments (216 and 237 MeV) a secondary emission monitor (SEM) was also installed downstream of the target location to provide an additional independent measurement of the total charge delivered to the target. A cross check of the normalizations of the two sets of data (200, 225, and 250 MeV) and (216 and 237 MeV) was performed using the $^{10}B(\vec{p},\pi^+)^{11}B$ reaction obtained for common energies and angles with both polarimeter systems. The agreement was better than 10% for both A_{N0} and yield.

The beam alignment and focusing of the beam on the target was accomplished by using two dipole bending magnets and a number of quadrupole magnets upstream of the target. The location and the size (typically 10×3 mm^2 XY) of the beam spot on the target was monitored at the beginning and at the end of each run with a multiwire beam monitor located at the target position. This monitor provided $\sim$0.5 mm accuracy. The beam polarization cycled through up, down, and off phases with a typical cycle of approximately 11 min.

B. The targets

Three different carbon targets were used in the present experiment. The 200, 225, and 250 MeV results were taken with a reactor grade graphite target of 162 mg/cm^2. The 216 and 237 MeV results were taken with research grade graphite of high uniformity and areal thickness of 93 and 45 mg/cm^2 for the forward and backward angles, respectively. The targets were mounted on a remotely controlled target ladder placed in a scattering chamber under beam line vacuum.

C. The spectrograph

The apparatus used to detect and identify the pions is shown in Fig. 1. The system is based on a 65 cm Browne-Buechner magnetic spectrograph.[24] Three scintillators (CE, C1, and C2) provided the fast trigger with the event defined as the following:

$$\text{Event} = \text{CE}\cdot\text{C1}\cdot\text{C2}\ .$$

The arrangement of the scintillators is shown in Fig. 1. The CE counter was 0.8 mm thick having a shape optimized for timing and constructed to the same dimensions as the exit aperture of the spectrograph, thus greatly reducing the number of background events arising from scattered particles which traverse all the scintillator counters, but which do not pass through the spectrometer pole-face gap. The other two scintillators, C1 and C2, were each 6.3 mm thick and were assembled with a photomultiplier tube connected to each end. Pulse height as well as timing information were provided by these scintillators. The material used for all three scintillators was NE110.

Time-of-flight (TOF) information was obtained by starting a time to digital converter (TDC) clock with the event pulse (timed to a meantimer output from C1) and stopping it with the cyclotron rf pulse, signifying the ar-

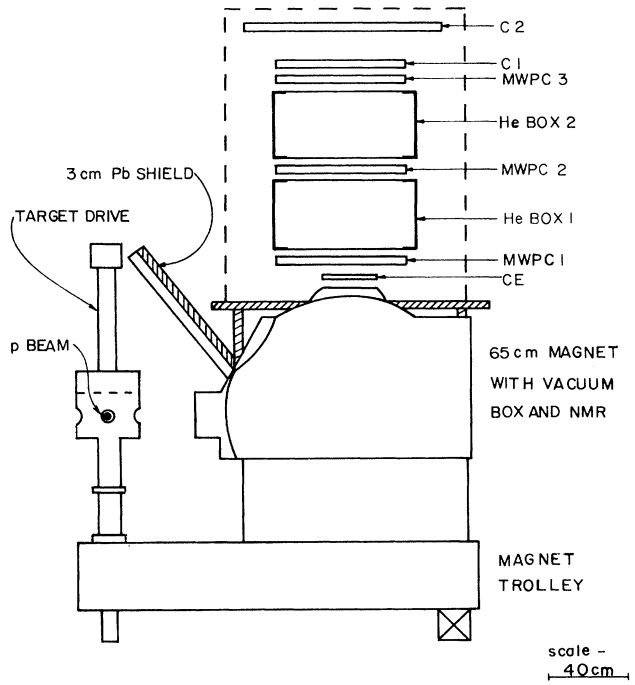

FIG. 1. Diagram of the pion detection system showing the magnetic spectrograph, the helically wound multiwire proportional chambers (MWPC's), and the scintillators providing the fast trigger (CE, C1, and C2).

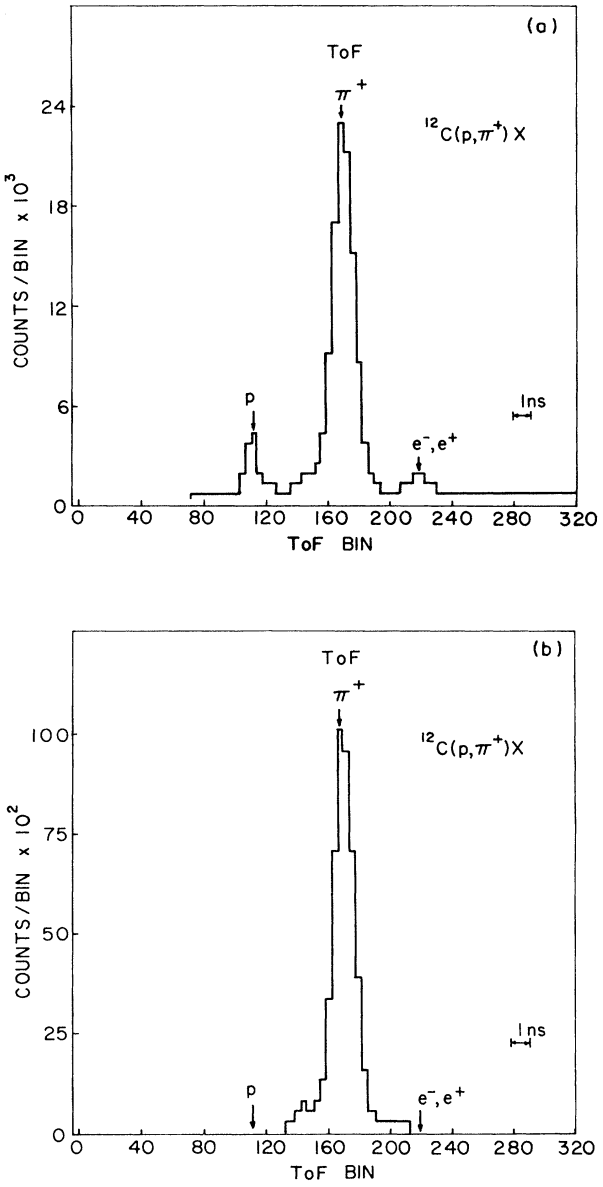

FIG. 2. Time-of-flight spectrum for $T_p=225$ MeV and $\theta_\pi(\text{lab})=46.5°$: (a) before data reduction and event-by-event analysis; (b) after event selection based on track reconstruction and imposition of cuts based on energy loss in the scintillators, but prior to application of TOF restrictions.

rival of the beam packet. A characteristic TOF spectrum obtained for $^{12}C(p,\pi^+)X$ is shown in Fig. 2(a). It is defined solely by the hardware logic, without any restrictions as to particle identification or track reconstruction, and thus it represents raw data. The events with longer TOF (smaller clock times) are consistent with protons scattered off the spectrograph vacuum box. Their intensity is angle dependent with the peak more pronounced at small spectrometer angles.

The particles with shorter TOF than the pions (larger clock times) are consistent with electrons or positrons following a direct path from the target to the scintillator. They are, most likely, generated by γ-ray conversion in the lead shielding surrounding the detectors. The flat background in Fig. 2(a) across the whole TOF spectrum is consistent with e^- or e^+ that have little correlation with the beam time structure; these events were observed to have a dE/dx smaller than that of the pions.

The pion trajectory and thus the pion momentum was defined by the value of the magnetic field and the information provided by the three helically wound multiwire proportional chambers (MWPC's).[25] The intercept of the particle trajectory along the focal plane was deduced by linear interpolation of position information from the three chambers. The use of three chambers provided a useful redundancy, enabling on-line determination of the absolute chamber efficiencies.

Pions were identified on the basis of the energy loss in the C1 and C2 scintillators, the TOF information, and the track reconstruction based on the MWPC information. In addition, in order to be accepted, a pion trajectory was required to satisfy a "colinear" condition imposed on the intercept information (x and y) from the three chambers. This colinearity requirement greatly reduced effects of $\pi\rightarrow\mu\nu$ decays occurring in the space between MWPC1 and MWPC3 and, combined with the track reconstruction, also reduced the flat TOF background by $\sim 95\%$.

Extrapolation of the nonbend plane component of the pion trajectory to the target provided an image of the beam spot on the target. This information also helped reduce the nonpion backgrounds as well as the spectra contamination due to pole-face scattered pions. Most of the pions scattered on the magnet pole faces lose some

momentum, and as a result, tend to contribute to a low energy tail associated with each peak. As a result of cuts placed on the target image width, only ~5% of the pions associated with a peak remain in the low energy tail.

D. Spectrograph calibration

The overall efficiency and acceptance of the spectrograph was calibrated relative to the $pp \rightarrow d\pi^+$ reaction. Rates were measured for the latter reaction at 400, 425, and 450 MeV and for various pion emission angles so as to cover the range of pion energies appropriate to the nuclear pion production program. The range of pion kinetic energy for which the instrument was suitable varied from ~30 MeV to a maximum of ~120 MeV (central rays). The upper limit was due to power supply and magnet coil limitations, whereas the lower limit was defined by the energy losses suffered while traversing the detector system.

A detailed knowledge of the line shape associated with the spectrograph was required for the determination of absolute cross sections. In order to determine this line shape, a scintillation counter was used to detect the deuteron in the $pp \rightarrow d\pi^+$ reaction while the pions were detected in the spectrograph. In such an arrangement pions generated in the $pp \rightarrow pn\pi^+$ breakup reaction are rejected resulting in a clean presentation of the line shape and the determination of the low energy tail associated with pole-face scattered pions.

From the above $pp \rightarrow d\pi^+$ rate measurements and the known $d\sigma/d\Omega$ the spectrograph effective solid angle was extracted and defined as the product of the geometrical solid angle $\Delta\Omega_0$ and the pion survival probability η, i.e.,

$$\Delta\Omega_{\text{eff}} = \Delta\Omega_0 \times \eta_{\pi - s} \ . \tag{1}$$

The empirical parametrization of the spectrograph based on the measurements of the $d\sigma/d\Omega$ for the $pp \rightarrow d\pi^+$ reaction applied to the measurement of $(d^2\sigma/d\Omega\, dE)$ and $A_{N0}(\theta)$ for the inclusive $^{12}C(\vec{p},\pi^+)X$ reaction is described elsewhere.[26] In addition a Monte Carlo simulation of the spectrograph was developed which helped resolve the various contributions to the acceptance as well as providing insight to the nature of the line shape.[27] This Monte Carlo code is an extension of that developed to analyze an earlier instrument at TRIUMF.[28]

III. RESULTS AND DISCUSSION

A. Data reduction

As stated earlier, pions were identified on the basis of energy loss in the C1 and C2 scintillators, track reconstruction based on MWPC information, and TOF restrictions. In order to reduce the effects of multiple scattering, $\pi \rightarrow \mu\nu$ decays, and pole face scattering, cuts were imposed on the track information. Figure 2(b) shows the effect of such cuts applied on the TOF spectrum for the case where no TOF cut was used on the run that generated Fig. 2(a). The reduction of the pion events from Figs. 2(a) to (b) reflects the effects of the various cut efficiencies as discussed below. The total background associated with nonpion events remaining after completion of a typical analysis corresponded to a cross section of less than 15 pb/MeV sr at 250 MeV, decreasing to less than 2 pb/MeV sr at 200 MeV due to improved dE/dx and TOF separation between pion and electrons at lower energies. The muon background has been estimated by the Monte Carlo analysis to be of the order of ~4%.

A representative pion energy spectrum for ^{12}C, after all cuts have been applied, is shown in Fig. 3. The overall energy resolution is ~800 keV, dominated by the spread in proton beam energy (~700 keV) characterizing the extracted beam. Multiple scattering, target thickness, and kinematic spread contributed ~400 keV FWHM.

The differential cross section was extracted from the experimental data through the relation[26]

$$\frac{d\sigma}{d\Omega} = \frac{Y\Gamma}{n_t n_p \eta_{ch} \eta_c \Delta\Omega_{\text{eff}} \eta_{XFP}} \ , \tag{2}$$

where Y is the area under the pion peak after background subtraction. Γ is an empirically defined tail correction parameter defined in terms of pion kinetic energy and peak integration limits in MeV. It is a correction factor accounting for the contribution of the low energy tail associated with each peak and extending under the other lower pion energy peaks in the pion spectra.[26,27] Γ was extracted from the $pp \rightarrow d\pi^+$ spectrograph calibration data. It was found to vary between 0.90 and 0.96 for this work. n_t is the number of target nuclei/cm^2. n_p is the total number of protons incident on the target as determined by polarimeter and SEM (where applicable). η_{ch} is the product of the efficiency values determined for each MWPC, i.e., $\eta_{ch} = \eta_1\eta_2\eta_3$, with η_1, η_2, and η_3 the absolute efficiencies for chambers 1, 2, and 3, respectively. The combined efficiency η_{ch} was typically between ~0.60 and ~0.70 for all runs. η_c is the combined efficiency of all the cuts applied to the peak area of interest and varied between ~0.40 and ~0.70 depending on the ^{13}C state under consideration. η_{XFP} is the focal plane efficiency, normalized to 1.00 for the middle of the focal plane. Since care was taken to place the ^{13}C states of interest in

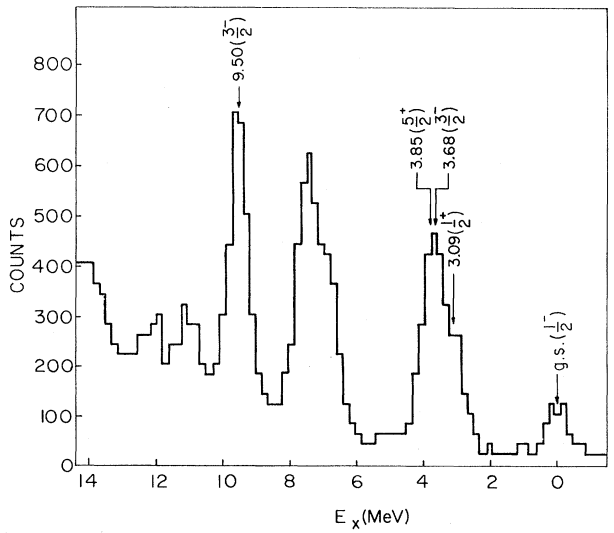

FIG. 3. Pion energy spectrum taken at $T_p = 237$ MeV, $\theta_\pi(\text{lab}) = 50°$. The figure represents only a portion of the available momentum acceptance of the spectrograph.

the focal plane region where the efficiency is relatively flat for the three MWPC's, η_{XFP} varied little in the ~ 0.99 to ~ 1.00 range. $\Delta\Omega_{\text{eff}}$ is defined in Eq. (1) and varied between 1.96 msr for 48 MeV pions and 2.21 msr for 98 MeV pions, the lowest and highest energy pions of interest, respectively. The empirical parameters Γ, η_c, η_{XFP}, and $\Delta\Omega_{\text{eff}}$ discussed above were extracted from the $pp \rightarrow d\pi^+$ calibration, whereas η_{ch} could be extracted from the experimental data due to the redundancy of MWPC information.

B. The results

The analyzing power $A_{N0}(\theta)$ and the spin-averaged (unpolarized) differential cross section $d\sigma/d\Omega(\theta)$ were calculated using the relations:

$$A_{N0}(\theta)=\frac{d\sigma(\uparrow)/d\Omega-d\sigma(\downarrow)/d\Omega}{P(\downarrow)d\sigma(\uparrow)/d\Omega+P(\uparrow)d\sigma(\downarrow)/d\Omega} \tag{3}$$

and

$$\frac{d\sigma}{d\Omega}(\theta)=\frac{P(\uparrow)d\sigma(\downarrow)/d\Omega+P(\downarrow)d\sigma(\uparrow)/d\Omega}{P(\uparrow)+P(\downarrow)}\,, \tag{4}$$

where P and $d\sigma/d\Omega$ are the magnitudes of the beam polarization and spin-dependent differential cross section, respectively. The arrows indicate the spin direction according to the Madison convention.[29] Background subtraction was performed assuming constant background under the $^{13}C_{\text{g.s.}}$ and $^{13}C^*_{3-4\text{ MeV}}$ states and by linearly interpolating the continuum on either side under the $^{13}C^*_{9.50\text{ MeV}}$ state, separating it from the pion continuum underneath.

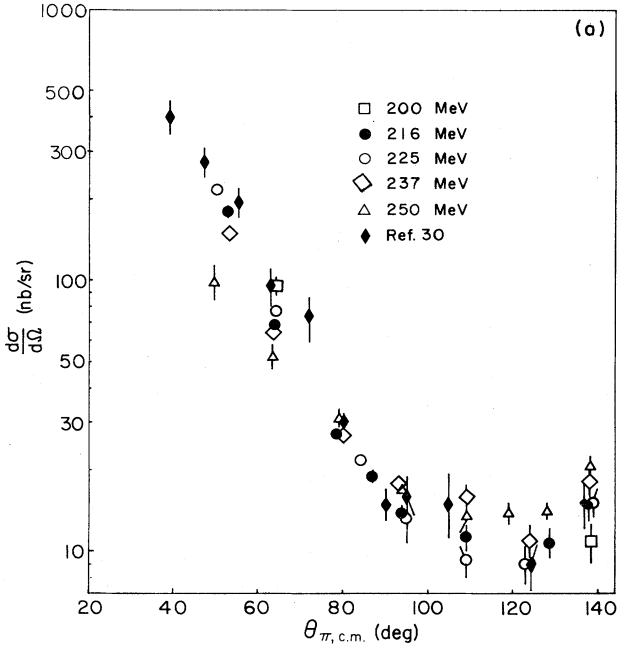

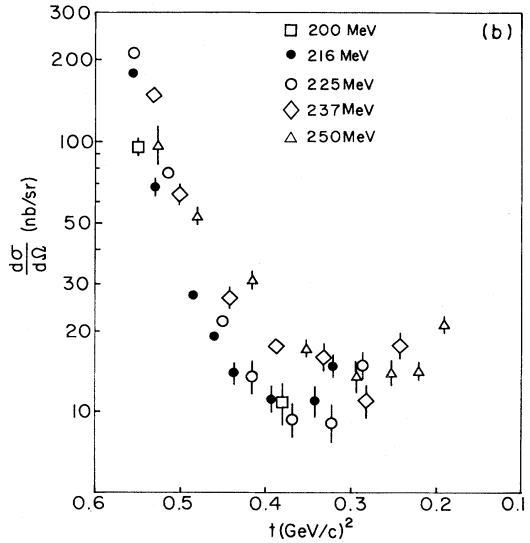

FIG. 4. The differential cross sections for the transition leading to the $^{13}C_{\text{g.s.}}$ (a) as a function of $\theta_{\pi,\text{c.m.}}$ and (b) as a function of the invariant four-momentum transfer t. In (a) the 200 MeV differential cross section results of Ref. 30 are also shown.

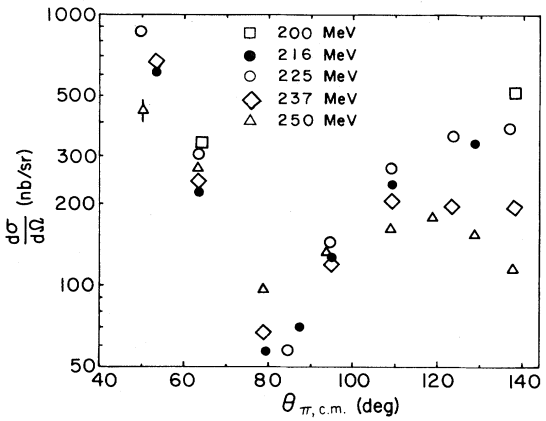

FIG. 5. The differential cross sections for the transition leading to the three unresolved states $^{13}C^*_{3.09,3.68,3.85\text{ MeV}}$.

The results are shown in Figs. 4–9 and are listed in Table I. In Fig. 4(a) the 200 MeV results from Refs. 30 and 8 are also presented in order to provide a more complete picture of the energy dependence of the differential cross section; at $\theta_{\text{c.m.}}=64°$ our results are in excellent agreement with those of Refs. 30 and 31. At $\theta_{\text{c.m.}}=138.2°$ our 200 MeV measurement is approximately 50% lower than the corresponding value in Ref. 30 (where the background posed a more severe problem than in this work). Our result is $\sim 40\%$ larger than the corresponding values reported in Ref. 31 where no evidence of backward peaking was observed. Our results, however, at 216 and higher energies indicate backward peaking as do the recent results of IUCF at 185 MeV.[32] It is not likely that the backward peaking evident at 185 and 216 MeV and higher energies does not exist at 200 MeV as well.

C. Sources of error

As noted at length in Sec. II D, the spectrograph effective solid angle was determined as a function of detected pion energy using the $pp \rightarrow d\pi^+$ reaction. Any uncertainty in the $pp \rightarrow d\pi^+$ differential cross section reflects itself as a compounding uncertainty in the spectrograph calibration. The cross section input data required for this cali-

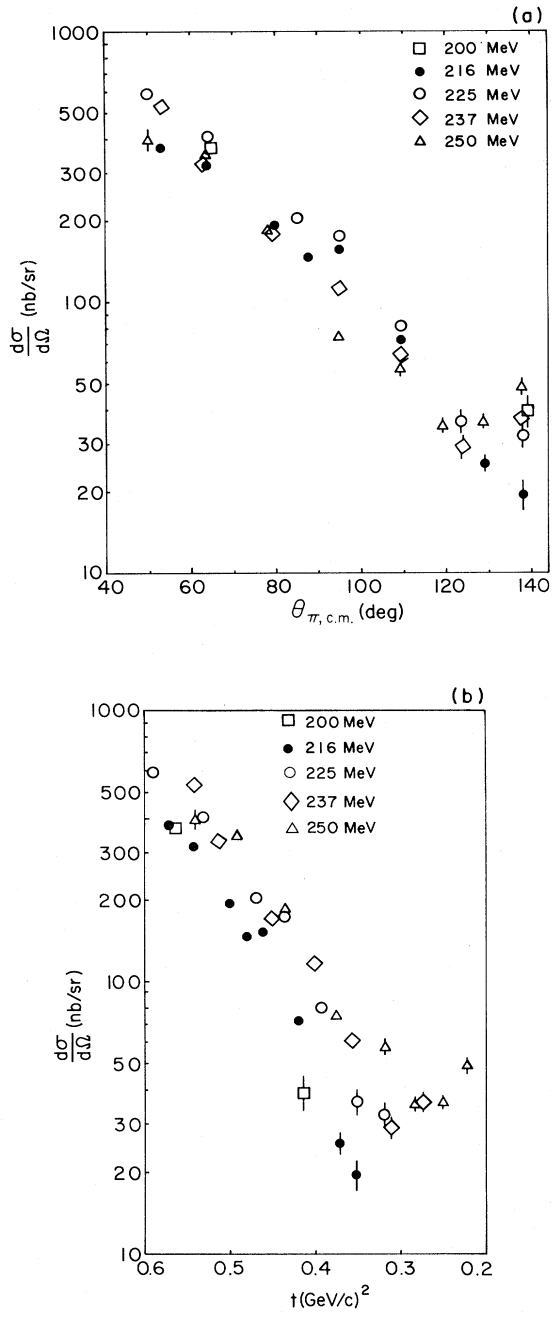

FIG. 6. The differential cross sections for the transition leading to the $^{13}C^{*}_{9.50\ MeV}$ state (a) plotted against $\theta_{\pi,c.m.}$ and (b) against t.

bration were taken from Refs. 33 and 34. At 450 MeV these references quote 1.33 and 1.57 mb, respectively, and an average of 1.45 mb was used. The uncertainty in the overall normalization is estimated as $\sim 10\%$.

For the 200, 225, and 250 MeV data the ^{12}C targets used were not as uniform in density as were the targets used for the 216 and 237 MeV data. As a result the quoted uncertainty in n_t is higher for the former set of data compared to that of the latter.

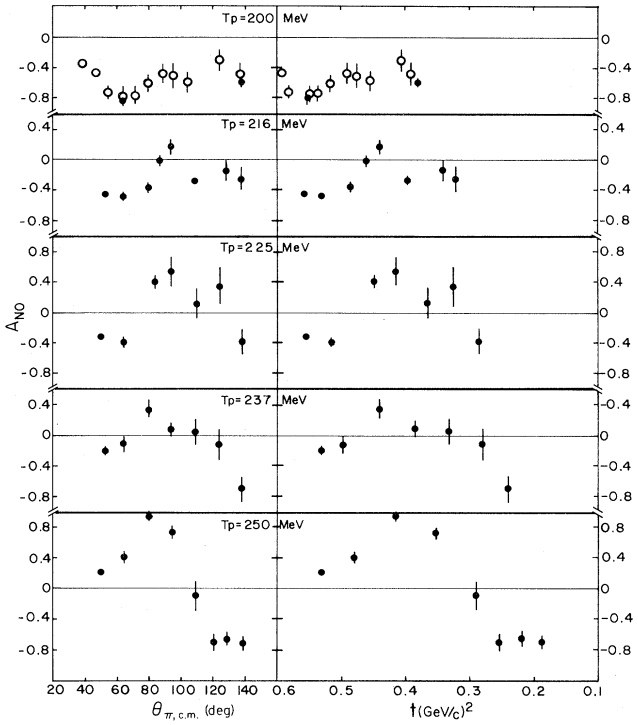

FIG. 7. The $A_{N0}(\theta)$ and $A_{N0}(t)$ are shown for the transition leading to the ground state. The open circles at $T_p = 200$ MeV are taken from Ref. 30.

The uncertainty in the total number of protons incident on the target, n_p, is also somewhat lower for the 216 and 237 MeV data compared to the 200, 225, and 250 MeV data. The reasons were the use of an improved polarimeter together with the use of an additional current monitor,

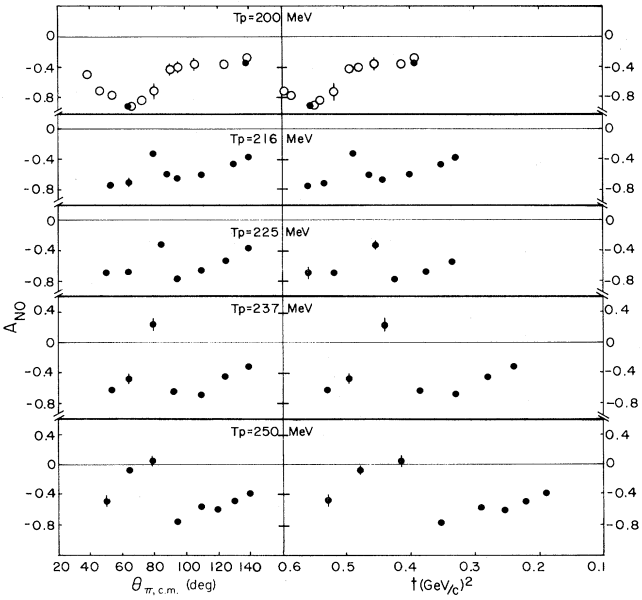

FIG. 8. As in Fig. 7 but for the transition leading to the unresolved $^{13}C_{3.09,3.68,3.85\ MeV}$ states. The open circles are from Ref. 30.

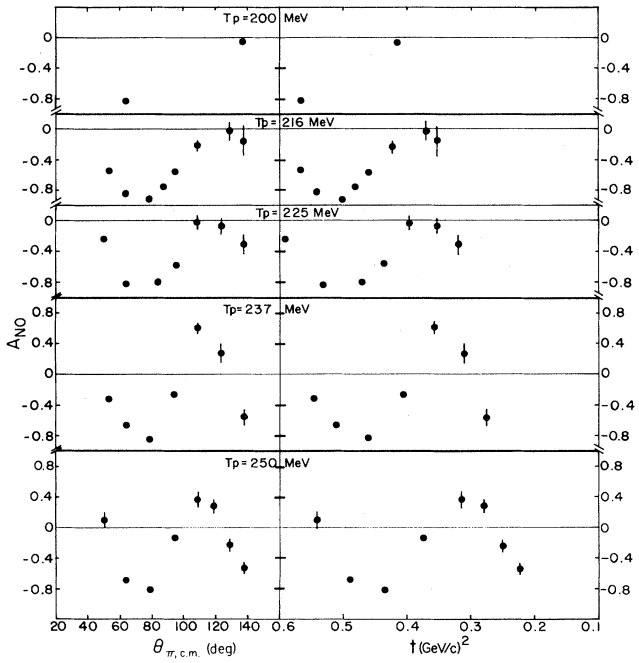

FIG. 9. As in Fig. 8 for the transition leading to the $^{13}C^*_{9.50\ MeV}$ state.

the SEM as indicated in Sec. II A. Every effort was made in all the data taking runs to position the beam spot in the center of the thin polarimeter CH_2 target. This minimizes the variation in the target effective areal density caused by the unavoidable wrinkling of the polyethylene material under the heat generated by the beam passing through the target material. The polarimeter was in a straight segment of beam line with two beam profile monitors, one upstream and the other downstream of the polarimeter; the beam spot location was therefore known to ~ 1.5 mm precision on the polarimeter target. Visual inspection of the target at the end of the pion production runs also verified the localized beam spot burn mark on the CH_2 foil. Where the SEM was present, the agreement between SEM and polarimeter was excellent with variation never exceeding 5% as a function of time and beam line tune for a given proton energy.

The systematic uncertainty in the beam polarization P is mainly due to the systematic error in the determination of the analyzing power of the polarimeter used and the energy in question. It is a small component in the 2—4 % range.[22]

The sources of systematic errors are summarized in Table II. An overall systematic uncertainty of $\sim 20\%$ is estimated for the 200, 225, and 250 MeV data and the total uncertainty due to systematic errors for the 216 and 237 MeV data is estimated at $\sim 15\%$. An overall relative uncertainty of $\sim 15\%$ has been estimated due to the uncertainty in the effective solid angle, the cut efficiencies, and the background subtraction.[26]

D. Discussion

As can be seen in Fig. 4(a), the $d\sigma/d\Omega$ for the $^{13}C_{g.s.}$ transition exhibits very little energy dependence as a function of $\theta_{c.m.}$, except at forward angles where $d\sigma/d\Omega$ decreases with increasing T_p. When considered as a function of four-momentum transfer squared, t, however [as in Fig. 4(b)], one observes that the differential cross section at lower momentum transfers ($T \simeq 0.5$ GeV$^2/c^2$) has peaked at the region of 225—237 MeV, while the slope of the forward angle cross sections gradually decreases with increasing proton energy. It would be of interest to investigate whether such behavior also extends to lower momentum transfers. While the differential cross sections for the transition leading to the $^{13}C_{g.s.}$ do not exhibit any significant variations in shape, other than the shape dependence noted above, the corresponding A_{N0} show a pronounced dependence on incident proton energy as observed in Fig. 7. For $T_p = 200$ MeV our A_{N0} results are in excellent agreement with those of Refs. 8 and 30. The observed energy dependence suggests a progressive change of shape for A_{N0} for proton energies between 200 and 250 MeV, a feature that was not apparent when the first measurements as a function of energy were reported.[18] When considered as a function of four-momentum transfer, t, the positive maximum of the analyzing power is centered around 0.4 (GeV/c)^2 and is surprisingly independent of beam energy.

In a shell model description the $^{13}C_{g.s.}$ is best described by a single particle (sp) state. On the other hand the $^{13}C^*_{9.50\ MeV}$ state is a two-particle—one-hole state (2p-1h). The differential cross sections for the transition leading to the latter state are shown in Fig. 6. In this case the cross section is essentially a simple exponential as a function of $\theta_{c.m.}$ although again there appears to be evidence of backward peaking with increasing energy. Again as was observed for the $^{13}C_{g.s.}$, it seems that the differential cross section, at low four-momentum transfer, has peaked at ~ 237 MeV. In most other respects, however, the situation for the two states is quite different. The A_{N0} for the $^{13}C^*_{9.50\ MeV}$ case (Fig. 9) shows the same characteristic shape, throughout the entire energy range, that has been observed for most nuclear pion production at 200 MeV and below. Here the *shape* of the A_{N0} is basically independent of incident energy when considered as a function of $\theta_{c.m.}$, whereas as a function of the four-momentum squared, t, the magnitude and the location of the A_{N0} minimum shifts from $t \simeq 0.510$ at 216 MeV to $t \simeq 0.430$ (GeV/c)^2 at 250 MeV. Any conclusions to be drawn from the results in Figs. 5 and 8 are hampered by the fact that the peak in Fig. 3 at 3—4 MeV of excitation is a composite of three transitions leading to the $^{13}C^*_{3.09\ MeV}$ (sp), $^{13}C^*_{3.68\ MeV}$ (2p-1h), and $^{13}C^*_{3.85\ MeV}$ (sp) states. It is clear from Fig. 8 that at least one of three states exhibit a dynamic behavior very similar to that of the $^{13}C_{g.s.}$, shown in Fig. 7. It is tempting to assume that the two single particle states are behaving like the $^{13}C_{g.s.}$ while the $^{13}C^*_{3.68\ MeV}$ (2p-1h) state shows similar characteristics as the $^{13}C^*_{9.50\ MeV}$ (2p-1h) state. Such a combined behavior would not be inconsistent with the observed dependence of A_{N0} as a function of incident proton energy shown in Fig. 8.

Where comparisons with other published data are possible the agreement with our results is good. For the $^{13}C_{9.50\ MeV}$ state the results of IUCF at $\theta_{c.m.} = 64°$ and

TABLE I. A list of the values for the differential cross sections and analyzing powers for the $^{12}C(\vec{p},\pi^+)$ reaction for transitions leading to the $^{13}C_{g.s.}$, $^{13}C^*_{3.09,3.68,3.85\ MeV}$, and $^{13}C^*_{9.50\ MeV}$ states. The numbers in parentheses reflect statistical uncertainties. Systematic errors are estimated as 19% for the 200, 225, and 250 MeV results and 14% for the 216 and 237 MeV.

	$^{12}C(\vec{p},\pi^+)^{13}C_{g.s.}$			$^{12}C(\vec{p},\pi^+)^{13}C^*_{3.09,3.68,3.85\ MeV}$			$^{12}C(\vec{p},\pi^+)^{13}C^*_{9.50\ MeV}$		
T_p (MeV)	θ (deg)	$d\sigma/d\Omega$ (nb/sr)	A	θ (deg)	$d\sigma/d\Omega$ (nb/sr)	A	θ (deg)	$d\sigma/d\Omega$ (nb/sr)	A
200	64.0	95.8(6.2)	−0.795(0.07)	64.1	330.3(11.7)	−0.917(0.03)	64.3	368.7(14.7)	−0.812(0.04)
	138.2	10.8(2.0)	−0.593(0.3)	138.3	523.5(9.1)	−0.346(0.02)	138.4	39.3(5.6)	−0.062(0.21)
216	53.4	179.9(5.6)	−0.436(0.03)	53.4	614.2(8.8)	−0.740(0.03)	53.6	369.2(9.6)	−0.537(0.03)
	63.8	68.6(3.9)	−0.470(0.09)	63.9	22.2(7.1)	−0.703(0.05)	64.0	317.(9.7)	−0.841(0.04)
	79.2	27.2(1.1)	−0.373(0.05)	79.3	57.9(1.7)	−0.349(0.03)	79.4	194.(3.6)	−0.925(0.02)
	87.3	19.1(1.0)	−0.027(0.07)	87.4	70.4(1.8)	−0.601(0.03)	87.6	144.6(3.2)	−0.759(0.02)
	94.4	13.9(1.2)	0.170(0.11)	94.4	125.5(2.5)	−0.651(0.02)	94.6	154.7(3.2)	−0.564(0.20)
	109.2	11.2(1.3)	−0.303(0.20)	109.3	235.9(3.4)	−0.602(0.01)	109.4	72.3(2.8)	−0.226(0.50)
	128.5	10.8(1.5)	−0.149(0.17)	128.6	336.7(3.5)	−0.462(0.01)	128.7	25.6(2.2)	−0.027(0.11)
	138.0	14.9(1.9)	−0.269(0.16)	138.1	380.9(4.3)	−0.376(0.01)	138.0	19.5(2.6)	−0.171(0.20)
225	49.5	213.4(5.0)	−0.313(0.04)	49.7	864.8(11)	−0.684(0.04)	49.8	591.4(11.6)	−0.247(0.03)
	63.8	77.4(4.0)	−0.377(0.07)	63.8	307.8(7.6)	−0.645(0.03)	63.9	406.9(10.6)	−0.825(0.03)
	84.3	21.8(1.2)	0.404(0.08)	84.3	57.9(1.7)	−0.323(0.04)	84.4	203.7(3.4)	−0.799(0.02)
	94.3	13.6(1.9)	0.547(0.22)	94.4	145.1(4.3)	−0.773(0.03)	94.5	174.9(5.6)	−0.575(0.04)
	109.1	9.3(1.3)	0.124(0.22)	109.2	272.3(3.9)	−0.654(0.02)	109.3	80.3(3.2)	−0.021(0.07)
	123.7	9.0(1.5)	0.342(0.28)	123.7	367.8(5.1)	−0.541(0.02)	123.8	36.3(3.5)	−0.064(0.10)
	138.0	14.9(1.5)	−0.384(0.15)	138.0	381.6(5.2)	−0.369(0.02)	138.1	32.2(3.3)	−0.336(0.12)
237	53.3	149.1(6.1)	−0.200(0.05)	53.3	670(10.8)	−0.625(0.02)	53.4	528.9(11.5)	−0.323(0.03)
	63.7	64.2(4.5)	−0.116(0.10)	63.8	245.7(7.6)	−0.455(0.04)	63.8	328.5(10.0)	−0.660(0.04)
	79.1	27.2(2.1)	0.348(0.11)	79.2	67.2(3.2)	0.240(0.07)	79.3	170.8(4.9)	−0.842(0.03)
	94.3	17.5(0.9)	0.076(0.10)	94.3	131.5(2.3)	−0.639(0.02)	94.4	112.7(2.5)	−0.264(0.04)
	109.1	16.1(1.8)	0.035(0.16)	109.1	205.2(2.9)	−0.675(0.02)	109.2	61.5(2.4)	0.600(0.06)
	123.7	10.9(1.5)	−0.119(0.22)	123.7	196.1(3.5)	−0.451(0.02)	123.8	29.1(2.5)	0.273(0.12)
	138.0	17.7(1.7)	−0.696(0.12)	138.0	197.3(3.4)	−0.326(0.02)	138.1	36.5(2.5)	−0.573(0.10)
250	49.6	96.4(16)	0.210(0.20)	49.7	443.9(35.0)	−0.480(0.07)	49.7	400.(35)	0.106(0.10)
	63.7	52.8(3.5)	0.404(0.09)	63.8	272.2(7.2)	−0.075(0.04)	63.8	349.7(9.2)	−0.670(0.03)
	79.1	30.8(2.3)	0.942(0.09)	79.2	95.6(3.3)	0.048(0.05)	79.6	183.2(5.1)	−0.809(0.04)
	94.2	17.3(1.1)	0.753(0.10)	94.3	137.8(2.4)	−0.762(0.02)	94.4	75.7(2.1)	−0.143(0.04)
	109.1	13.5(1.8)	−0.111(0.20)	109.1	163.3(3.1)	−0.561(0.02)	109.2	57.6(3.2)	0.372(0.09)
	118.8	13.8(1.3)	−0.714(0.11)	118.9	180.1(2.4)	−0.587(0.02)	118.9	35.2(1.7)	0.275(0.07)
	128.4	14.1(0.8)	−0.668(0.08)	128.5	155.7(1.8)	−0.477(0.02)	128.5	35.9(1.6)	−0.249(0.07)
	138.0	21.1(1.6)	−0.271(0.08)	138.0	117.8(2.2)	−0.381(0.02)	138.0	48.3(2.5)	−0.539(0.06)

TABLE II. Sources of systematic errors and their assigned values.

Source	200, 225, and 250 MeV	216 and 237 MeV
Spectrograph calibration	10%	10%
Polarization P	~3%	~2%
n_t	3%	1%
n_p[a]	15%	10%
	Total ≈ 19%	Total ≈ 14%

[a]The relative (statistical) component is less than 1%.

~138° (Ref. 35) are in good agreement with our results shown in Fig. 6.

Although there has been significant improvement in recent years in the quantity and quality of experimental results for $A(p,\pi^{\pm})A+1$ pion production reactions, our understanding of the reaction mechanism is still limited. Recent theoretical work has been oriented towards developments involving microscopic TNM calculations. It is fortunate that such work is being carried out by a number of groups considering the complicated diagrams that have to be taken into account for reactions of this sort. Keister and Kisslinger (KK),[11] Iqbal and Walker (IW),[36] and Dillig and Conte (DC) (Ref. 12) all have computer codes either running or in the final stages of preparation. Differential cross section results from the KK code[37] are plotted in Fig. 10 for 200 MeV (KK200) and 250 MeV (KK250) and are compared to our experimental results.

The diagrams included in these calculations, based on an isobar-doorway model[38] are the direct (D), the exchange (E), and the plane wave Born approximation (B). The first two terms proceed through resonant terms (the Δ resonance) and therefore one would expect this model, as well as the IW and DC models, to be more relevant for incident proton energies appropriate to near on-shell Δ production.

In Fig. 10 the effect of the energy dependence of the Δ channel is manifested by the substantially higher differential cross section predicted at 250 MeV (KK250) compared to 200 MeV (KK200), a trend not reflected by the experimental data. The equivalent $A_{N0}(\theta)$ predictions are shown in Fig. 11. Thus Figs. 10 and 11 provide a good evaluation of the degree to which the KK calculations, at their present stage of development, are able to explain the energy dependence for both $d\sigma/d\Omega$ and A_{N0} results under identical inputs. The 250 MeV $A_{N0}(\theta)$ data are reproduced well by the model, whereas the $d\sigma/d\Omega$ predictions are in sharp disagreement with our data. For comparison, the IW model[36] underestimates the magnitude of the $d\sigma/d\Omega$ and introduces more structure in the angular distribution than our results indicate. In fact, our data lie between the predictions of these two models. The IW model[36,39] fares much better, however, in describing the angular dependence of the $d\sigma/d\Omega$ for the $^{13}C^{*}_{9.50\ MeV}$ transition, as shown in Fig. 12. In the forward angles the general features of the experimental results are reproduced well although in this case, as in the $^{13}C_{g.s.}$ transition, the magnitude of the $d\sigma/d\Omega$ is again underestimated and the

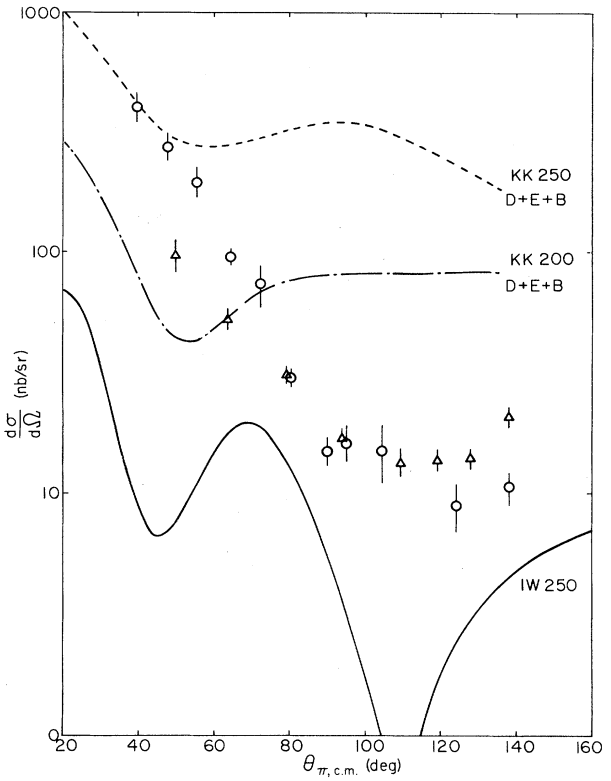

FIG. 10. Comparison of TNM microscopic calculations for the $^{12}C(p,\pi^{+})^{13}C_{g.s.}$ reaction with the results reported in this paper. The 200 MeV results are a combination of the results in Ref. 30 and the present measurements. The dash-dot curve represents $d\sigma/d\Omega$ calculated for 200 MeV, while the dotted curve is calculated for 250 MeV incident protons (Ref. 37). The solid line represents $d\sigma/d\Omega$ obtained from Ref. 36.

indication of backward peaking is not anticipated.

The recently discovered selectivity of the (p,π^{-}) reaction to stretched 2p-1h states[40] provides a fresh outlook in a reaction mechanism that can be very complicated

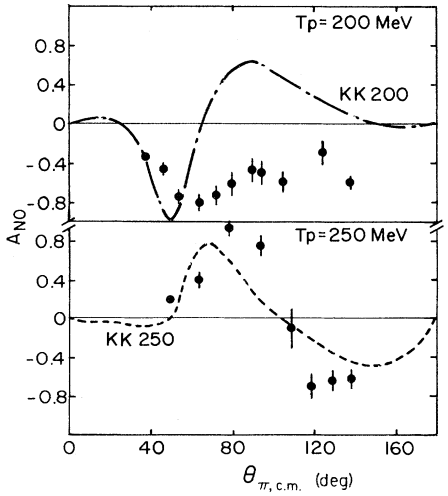

FIG. 11. Comparison of $A_{N0}(\theta)$ experimental results with the calculations of Ref. 37. The data and the theory are as explained in Fig. 10.

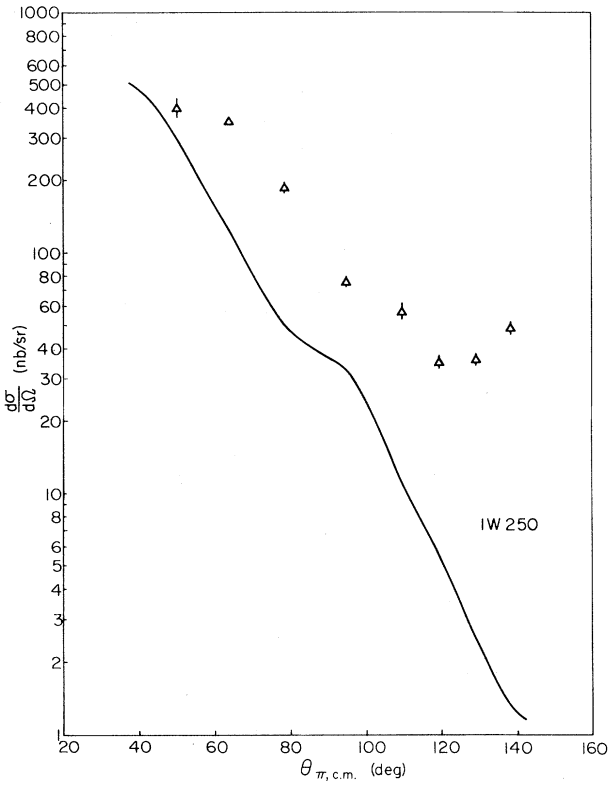

FIG. 12. Comparison of TNM microscopic calculations (Ref. 39) for the $^{12}C(p,\pi^+)$ $^{13}C^*_{9.50\ MeV}$ reaction with the results reported in this paper for 250 MeV incident protons.

indeed. In a TNM, and assuming no interaction involving three or more particles in the Hamiltonian, the (p,π^-) reaction can proceed via only one diagram each, in the direct and exchange terms, while in general the (p,π^+) reaction proceeds via a total of six possible diagrams. In the specific cases, however, of transitions leading to stretched neutron 2p-1h states (such as the $^{13}C_{9.50\ MeV}$ transition), the (p,π^+) reaction can only proceed via two diagrams, just as the (p,π^-) transition in general.[39] In principle then, comparisons with the $^{13}C^*_{9.50\ MeV}$ transitions should provide a simpler and better test of such theoretical models than comparisons to transitions leading to single particle states. It is hoped the results presented in this paper will spur further improvements in the models indicated above. For a recent overview of (p,π) systematics and updated references the reader is referred to Ref. 41.

IV. CONCLUSIONS

We have measured the differential cross sections and analyzing powers in the angular range 46°—135° in the laboratory frame and 200—250 MeV energy range for the $^{12}C(\vec{p},\pi^+)^{13}C$ reaction. Our data indicate significant variations in the angular dependence of A_{N0} as a function of incident energy for different transitions of ^{13}C. For the $d\sigma/d\Omega$ the energy dependence is different depending on whether small and large momentum transfers are considered. The cross section for the transitions leading to the $^{13}C^*_{g.s.}$ and $^{13}C^*_{9.50\ MeV}$ states peak at $T_p \simeq 237$ MeV for $t \simeq 0.550$ $(GeV/c)^2$. For larger momentum transfer, however, the differential cross section shows an increase with incident energy, as one would expect in a reaction mechanism dominated by the formation in the intermediate state of a Δ isobar. On the other hand the role of the Δ in nuclear pion production has not been explored with the same quality and quantity of data that have been accumulated at energies well below and well above the Δ region of $\sim$325 MeV. Good resolution experiments on selected nuclei are still needed in the 200—400 MeV region. Experiments that will provide both (p,π^+) and (p,π^-) data leading to specific final states (especially those with a simple description within the TNM such as stretched 2p-1h states) are important. Angular distributions at or near energies for the on-shell production of the (3,3) resonance, as well as total cross section measurements as a function of momentum transfer, are also needed.

ACKNOWLEDGMENTS

The assistance of Mrs. D. Sample in the data handling and analysis is very much appreciated. One of the authors (G.J.L.) especially acknowledges the very useful discussions with Dr. B. D. Keister and in particular his willingness to share the results of his (p,π) code in the 200—250 region as soon as they came out in print form. This work was supported in part by a National Science Energy Research Council (NSERC) grant.

*Present address: Department of Physics and Astronomy, University of Regina, Regina, Saskatchewan, Canada S4S 0A2.

†Permanent address: Physics Department, University of Manitoba, Winnipeg, Manitoba, Canada R3T 2N2.

‡Permanent address: Physics Department, James Cook University of North Queensland, Townsville, North Queensland, Australia.

[1]B. Hoistad, in *Advances in Nuclear Physics,* edited by J. W. Negele and E. Vogt (Plenum, New York, 1979), Vol. 11, p. 135.

[2]D. F. Measday and G. H. Miller, Ann. Rev. Nucl. Part. Sci. **29**, 121 (1979).

[3]H. W. Fearing, in *Progress in Particle and Nuclear Physics,* edited by D. Wilkinson (Pergamon, New York, 1981), Vol. 7, p. 113.

[4]S. Dahlgren, P. Grafstrom, B. Hoistad, and A. Åsberg, Nucl. Phys. **A204**, 53 (1973).

[5]S. Dahlgren, P. Grafstrom, B. Hoistad, and A. Åsberg, Nucl. Phys. **A211**, 243 (1973).

[6]S. Dahlgren, P. Grafstrom, B. Hoistad, and A. Åsberg, Nucl. Phys. **A227**, 245 (1974).

[7]S. Dahlgren, P. Grafstrom, B. Hoistad, and A. Åsberg, Phys. Lett. **47B**, 439 (1973).

[8]E. G. Auld, A. Haynes, R. R. Johnson, G. Jones, T. Masterson, E. L. Mathie, D. Ottewell, P. Walden, and B. Tatischeff, Phys. Rev. Lett. **41**, 462 (1978).

[9]G. Jones, in *Meson-Nuclear Physics-1979 (Houston),* Proceedings of the 2nd International Topical Conference on Meson-Nuclear Physics, AIP Conf. Proc. No. 54, edited by E. V. Hungerford III (AIP, New York, 1979), p. 116.

[10]M. C. Tsangarides, Ph.D. thesis, Indiana University, 1979 (unpublished).

[11]L. S. Kisslinger, University of Washington Report 40048-82-NT2, 1982; in *Pion Production and Absorption in Nuclei—1981 (Indiana University Cyclotron Facility),* Proceedings of the Conference on Pion Production and Absorption in Nuclei, AIP Conf. Proc. No. 79, edited by R. D. Bent (AIP, New York, 1982), p. 243; B. D. Keister, *ibid.*, p. 265; B. D. Keister and L. S. Kisslinger, Nucl. Phys. **A412**, 301 (1984).

[12]M. Dillig, F. Soga, and J. Conte, in *Pion Production and Absorption in Nuclei—1981 (Indiana University Cyclotron Facility),* Proceedings of the Conference on Pion Production and Absorption in Nuclei, AIP Conf. Proc. No. 79, edited by R. D. Bent (AIP, New York, 1982), p. 275.

[13]T. P. Sjoreen, M. C. Green, W. W. Jacobs, R. E. Pollock, F. Soga, R. D. Bent, and T. E. Ward, Phys. Rev. Lett. **45**, 1769 (1980).

[14]T. P. Sjoreen, P. H. Pile, R. E. Pollock, W. W. Jacobs, H. O. Meyer, R. D. Bent, M. C. Green, and F. Soga, Phys. Rev. C **24**, 1135 (1981).

[15]M. C. Green, in *Pion Production and Absorption in Nuclei—1981 (Indiana University Cyclotron Facility),* Proceedings of the Conference on Pion Production and Absorption in Nuclei, AIP Conf. Proc. No. 79, edited by R. D. Bent (AIP, New York, 1982), p. 131.

[16]G. J. Lolos, E. L. Mathie, P. L. Walden, G. Jones, E. G. Auld, and R. B. Taylor, Phys. Rev. C **25**, 1082 (1982).

[17]E. G. Auld, G. Jones, G. J. Lolos, E. L. Mathie, P. L. Walden, and R. B. Taylor, Phys. Rev. C **25**, 2222 (1982).

[18]G. J. Lolos, P. L. Walden, E. L. Mathie, G. Jones, E. G. Auld, W. R. Falk, and R. B. Taylor, Phys. Rev. C **25**, 1086 (1982).

[19]G. J. Lolos, in *Pion Production and Absorption in Nuclei—1981 (Indiana University Cyclotron Facility),* Proceedings of the Conference on Pion Production and Absorption in Nuclei, AIP Conf. Proc. No. 79, edited by R. D. Bent (AIP, New York, 1982), p. 201.

[20]G. J. Lolos, G. Jones, E. G. Auld, W. R. Falk, G. Giles, E. L. Mathie, B. McParland, P. L. Walden, and W. Ziegler, Nucl. Phys. **A386**, 477 (1982).

[21]D. V. Bugg, J. A. Edgington, C. Amsler, R. C. Brown, C. J. Oram, K. Shakarchi, N. M. Stewart, G. A. Ludgate, A. S. Clough, D. Axen, S. Jaccard, and J. Vávra, J. Phys. G **4**, 1025 (1978).

[22]L. G. Greeniaus and J. Soukup, TRIUMF Internal Report TRI-DNA-81-1, 1981.

[23]D. A. Hutcheon (private communication).

[24]C. P. Browne and W. W. Buechner, Rev. Sci. Instrum. **27**, 899 (1959).

[25]D. M. Lee, S. E. Sobottka, and H. A. Thiessen, Nucl. Instrum. Methods **120**, 153 (1974).

[26]W. R. Falk, E. G. Auld, G. Giles, G. Jones, G. J. Lolos, W. Ziegler, and P. L. Walden, Nucl. Phys. A (unpublished).

[27]W. Ziegler, M.Sc. thesis, University of British Columbia, 1983 (unpublished).

[28]E. L. Mathie, G. Jones, T. Masterson, D. Ottewell, P. L. Walden, E. Auld, A. Haynes, and R. R. Johnson, Nucl. Phys. **A397**, 447 (1983).

[29]*Proceedings of the 3rd International Symposium on Polarization Phenomena in Nuclear Reactions, Madison, 1970,* edited by H. H. Barschall and W. Haeberli (University of Wisconsin, Madison, 1971).

[30]E. L. Mathie, Ph.D. thesis, University of British Columbia, 1980 (unpublished).

[31]B. Hoistad, P. H. Pile, T. P. Sjoreen, R. D. Bent, M. C. Green, and F. Soga, Phys. Lett. **94B**, 315 (1980).

[32]R. D. Bent (private communication).

[33]C. Richard-Serre, W. Hirt, D. F. Measday, E. G. Michaelis, M. J. M. Saltmarsh, and P. Starek, Nucl. Phys. **B20**, 413 (1970).

[34]G. Jones, in *Pion Production and Absorption in Nuclei—1981 (Indiana University* Cyclotron Facility), Proceedings of the Pion Production and Absorption in Nuclei, AIP Conf. Proc. No. 79, edited by R. D. Bent (AIP, New York, 1982), p. 15.

[35]IUCF Annual Report, 1980, p. 127.

[36]M. J. Iqbal, Ph.D. thesis, Indiana University, 1982 (unpublished).

[37]B. D. Keister (private communication); for a detailed explanation of the terms involved in these calculations see Keister and Kisslinger, Ref. 11.

[38]L. S. Kisslinger and W. L. Wong, Am. J. Phys. **99**, 374 (1976).

[39]M. J. Iqbal and G. E. Walker (private communication).

[40]S. E. Vigdor, T. G. T. Throwe, M. C. Green, W. W. Jacobs, R. D. Bent, J. J. Kehayias, W. K. Pitts, and T. E. Ward, Phys. Rev. Lett. **49**, 1314 (1982).

[41]P. L. Couvert, University of Alberta/TRIUMF Workshop on Studying Nuclei with Medium Energy Protons, Edmonton, 1983, TRIUMF Report TRI-83-3, edited by J. M. Greben, p. 287.